# Initial growth stage of nano-scaled TiN films: Formation of continuous amorphous layers and thickness-dependent crystal nucleation

T. Q. Li [a)], S. Noda [a)], and H. Komiyama

*Department of Chemical System Engineering, University of Tokyo, 7-3-1 Hongo, Bunkyo-ku, Tokyo 113-8656, Japan*

T. Yamamoto

*Department of Advanced Materials Science, University of Tokyo, 7-3-1 Hongo, Bunkyo-ku, Tokyo 113-8656, Japan*

Y. Ikuhara

*Department of Material Science, University of Tokyo, 7-3-1 Hongo, Bunkyo-ku, Tokyo 113-8656, Japan*

(Received

[a)]Author to whom correspondence should be addressed; electronic mail: litg@chemsys.t.u-tokyo.ac.jp; noda@chemsys.t.u-tokyo.ac.jp

The initial growth stage of titanium nitride (TiN) deposited by reactive magnetron dc sputtering onto (111)-oriented Si substrates was investigated by using high-resolution transmission electron microscopy (HRTEM). During the initial growth stage, a continuous amorphous layer was observed when the deposited film was less than 1 nm thick. Crystal nucleation occurred from the amorphous layer when the film grew to about 2 nm thick. No preferred orientation was found for the initial crystal nuclei. The growth of the crystal grains depended on the $N_2$ partial pressure, $P_{N2}$. Increasing $P_{N2}$ from 0.047 to 0.47 Pa enhanced lateral grain-growth and coalescence between grains. For $P_{N2}$ = 0.47 Pa, planar grains with large lateral dimension were found formed by grain-growth and coalescence, inducing a (200) film orientation. For films formed at $P_{N2}$ = 0.47 Pa, an amorphous interlayer 1.5-1.8 nm thick formed between TiN layer and Si substrate, and was indicated to be primarily $SiN_x$ by XPS and HRTEM. This interlayer was less than 0.5 nm thick in films formed at $P_{N2}$ = 0.047 Pa.

PACS numbers:

1. 68.55.Ac.

2. 68.55.Jk.

3. 81.15.Cd.

## I. INTRODUCTION

Titanium nitride (TiN) thin films are widely used for a variety of structural and electronic applications. Previous research on TiN thin films focused on the textural evolution of TiN films hundreds of nanometers thick, which have anisotropic properties (e.g., elasticity and diffusion resistance). For example, a strongly (111) textured TiN under-layer induces a strongly (111) textured Al upper-layer that has a longer electromigration life compared with other textured Al metal lines. [1-3] The textural evolution mechanisms have been explained from the viewpoints of thermodynamics and kinetics. [4-8] Recently, efforts were made to quantitatively model the homogeneous TiN growth process, such as two-dimensional island coarsening and decay processes on (111) or (200) single crystal TiN surfaces. [9-11]

As the packing density of the ultra large-scale integrated (ULSI) devices increases and the characteristic feature size decreases to nanometer-size regime, the thickness of diffusion barriers (e.g., TiN and TaN) used for metal interconnect (e.g., Al and Cu) is expected to be reduced to less than 10 nm.[12] For such thin films, besides the film texture, factors such as grain-size and growth mode play even more important roles in film performances. For example, Patsalas et al [13] found that a quasi-2D growth on GaN results in a much lower TiN film resistivity compared with a 3D growth on Si, in the film thickness range of 4 ~ 14 nm. To control structural and material properties of such thin films, a detailed understanding of their initial growth mechanisms is needed.

However, except for the large volume of investigations on homogeneous TiN growth, little effort has been made to clarify the initial stage of the non-epitaxial heterogeneous growth of TiN. [8, 13, 14] which is important for designing film-growth processes for practical applications.

Transmission electron microscopy (TEM) is a direct and effective method to determine film morphology. In this work, high-resolution transmission electron microscopy (HRTEM) and nano-beam diffraction (NBD) techniques were used to investigate, in detail, the initial growth

stage of TiN on (111) Si, from sub-nanometer to nanometer-order thickness. To our surprise, the film was initially formed as a continuous amorphous layer. As the film grew, crystallization occurred from the amorphous layer with no preferred orientation. The grain-growth process was affected by the $N_2$ partial pressure, $P_{N2}$. Increasing $P_{N2}$ enhanced the lateral grain growth and coalescence, resulting in a larger lateral grain-size and inducing restructuring of the grains to thermodynamically favored (200) orientation.

## II. EXPERIMENT

TiN thin films were reactive sputter-deposited with a Ti target in an $N_2$/Ar atmosphere by using a magnetron sputtering system equipped with dc and rf power sources. The system is described in detail elsewhere, [8] and only the main features are described here. The sputter chamber had a base pressure of $5\times10^{-6}$ Pa. The target was a 2-inch-diameter, 99.99% pure Ti disc. Before being loaded, the wafers were treated chemically in a mixture of concentrated sulphuric acid and $H_2O_2$, and then dipped into a 1% HF solution to remove the contaminants and the native $SiO_2$ layer on the surface. Before deposition onto substrates, the target was pre-sputtered for 5 min under the same conditions as for TiN deposition. TiN deposition was done without substrate heating. No bias voltage was applied to the substrates and the substrate self bias potentials induced from the plasma were –23.0 V at $P_{N2}$ = 0.047 Pa and -29.3 V at $P_{N2}$ = 0.47 Pa, respectively. The sputtering gases, $N_2$ and Ar, were controlled with independent mass-flow controllers, and mixed before they were introduced into the sputter chamber. The total pressure, $P$, in the sputtering chamber was maintained at $P$ = 0.93 Pa and the total flow rate, $F$, was maintained at $F$ = 20 sccm. The substrate-to-target distance was 50 mm, and the discharge power to the Ti target was dc 69 W. To avoid film oxidation in air and to immobilize the deposits on the surface against irradiation of the electron beam during observation by transmission electron microscopy (TEM), for samples used for TEM

observation a 10 nm $SiO_2$ layer was deposited immediately after TiN deposition.

To determine the deposition rates, the film thickness was measured with a stylus profilometer (KLA-Tencor P-10). The thickness of initial growth samples was calculated from the deposition rate and time, which we refer to in this paper as "$l_c$".

The texture of 50 nm thick films was evaluated with x-ray diffraction (XRD) (Rigaku RINT2400) by using CuKα radiation. The microstructure of nano-scale films was evaluated from both plan-view and cross-sectional HRTEM images, selected area electron diffraction (SAED) and NBD analysis by using an FETEM (JEOL, JEM2010F) operated at 200 kV. The film composition was determined with in situ Auger electron spectroscopy (AES). Ex-situ depth profiling of elemental composition for 20 nm thick TiN films was done by using x-ray photoelectron spectroscopy (XPS) (PHI 1600) with an Mg Kα source and a 3 keV argon-ion beam source for sputter etching.

## III. EXPERIMENTAL RESULTS

### A. Deposition conditions for investigating initial growth stage

We determined the deposition conditions needed to obtain stoichiometric TiN films with good crystallinity, by varying $P_{N2}$ from 0.015 Pa ≤ $P_{N2}$ ≤ 0.47 Pa. Increasing $P_{N2}$ from 0.015 to 0.47 Pa caused the preferred orientation of the films to change from TiN (111) to TiN (200). [8] AES results indicate that the Ti/N ratio was 1:1 in this pressure range. We grew films at $P_{N2}$ = 0.047 Pa (Condition I) and $P_{N2}$ = 0.47 Pa (Condition II) (see Table I) to investigate the initial growth stage. Under Conditions I and II the films had complete (111) and (200) preferred orientations, respectively, at film thickness of 50 nm. The growth rates were determined to be 0.19 and 0.063 nm/s under these two conditions (see Table I).

### B. Formation of initial continuous amorphous layers and thickness-dependent crystal

**nucleation**

Figs. 1 and 2 show plan-view HRTEM images together with corresponding SAED patterns and cross-sectional HRTEM images of TiN films deposited under Condition I (Figs. 1a-c and 2a-c), and under Condition II (Figs. 1d-f and 2d-f). Fig. 1a shows a film deposited for 4 s under Condition I, resulting in an $l_c$ of 0.8 nm. Fig. 1d shows a film deposited for 10.5 s under Condition II, resulting in an $l_c$ of 0.7 nm. The absence of crystal grains in the plan-view images and the absence of crystalline diffraction peaks in corresponding SAED patterns indicate that the films were amorphous. The cross-sectional images shown in Figs. 2a and 2d also indicate that the films were continuous and amorphous.

Figs. 1b, 1e, 2b, and 2e show that crystal grains existed inside the 2-nm-thick films deposited for 10 s under Condition I and for 30 s under Condition II, and were identified from their lattice constants as TiN crystal grains. As shown by the SAED patterns, the 2-nm-thick films deposited under both conditions had no preferred orientation.

The SAED patterns and HRTEM images shown in Figs. 1c, 1f, 2c, and 2f indicate that the films deposited for 30 s under Condition I and for 60 s under Condition II became typical polycrystalline films with mixed crystal orientations.

To further confirm the transition from amorphous to crystalline structures in the films, NBD measurements, made with a probe size of about 0.7 nm, were used to identify the crystal structure in the film. Fig. 3a shows a NBD pattern obtained from inside a film deposited for 4 s under Condition I, which indicates a hollow pattern resulting from an amorphous film. The faint patterns superimposed on the hollow pattern were due to the silicon substrate, because the edge of the probe slightly overlapped at the film/substrate interface. Figs. 3b and 3c show NBD patterns obtained from Si substrates and from the crystallized film deposited for 10 s under Condition I, respectively. In Fig. 3c, the diffraction spots correspond to B1 NaCl-type TiN crystals with TiN (111), (200), and (220) planes. The faint patterns superimposed on the

main patterns were also due to the silicon substrate.

The thickness of the film measured from the cross-sectional HRTEM images deposited for 4 s under Condition I and for 10.5 s under Condition II were 1.6 and 1.3 nm, respectively, which is about twice as thick as the calculated film thickness, $l_c$. This may be due to the lower density of the initial amorphous layer compared with its crystal phase. On the other hand, films deposited for 10 s under Condition I and for 30 s under Condition II were 2.0 nm thick, almost the same as the $l_c$ of 1.9 nm.

### C. Grain growth and coalescence process

Fig. 4 shows histograms of the frequency of occurrence of TiN grains versus ~~various~~ lateral grain sizes. For each operating condition, the histogram was obtained from the measurement of the size of more than 100 randomly-sampled grains from plan-view TEM images. Fig. 4a shows the grain size for films deposited under Condition I, which indicates that as the deposition time increased from 10 s ($l_c$ = 2 nm) to 30 s ($l_c$ = 6 nm), the average lateral grain size increased from 3.0 to 4.2 nm. Fig. 4b shows the grain size for films deposited under Condition II, which indicates that as the deposition time increased from 32 s ($l_c$ = 2 nm) to 60 s ($l_c$ = 4 nm), the average grain size increased from 3.7 to 4.8 nm. To correlate the grain growth to film thickness for Conditions I and II, Fig. 5 shows a correlation of the lateral grain size with the film thickness, and indicates that the lateral grain size of the film deposited under Condition II were larger than that deposited under Condition I. For Condition II, the grain lateral size was still larger than the grain height up to a film thickness of 4 nm.

In the 4-nm film deposited under Condition II, about 15% of the grains had a coalesced shape and relatively large lateral size (7-10 nm). All these grains with relatively large lateral size were (200) oriented. In Fig. 1f, several grains with a coalesced shape and large lateral size are indicated by arrows and numbered, and lattice imaging shows that these grains were

(200) oriented. Fig. 6 shows enlarged images of these grains, together with four grains from Fig. 1c that were formed during 30-s deposition under Condition I.

### D. Interlayer formation under high $N_2$ partial pressure

For films deposited under Condition II (see Figs. 2d-f), a 1.5-1.8 nm thick amorphous interlayer formed between the deposits and the Si substrate, and changed little with film growth, whereas for films deposited under Condition I, the amorphous interlayer thickness was less than 0.5 nm (see Figs. 2a-c). The independence of the interlayer thickness on film thickness means that the amorphous interlayer was formed during the initial deposition stage.

To investigate compositions of the initial layer and layer/substrate interface, ex situ XPS depth profiling was made for Ti 2p, N 1s, Si 2p, and O 1s peaks. Fig. 7 shows the depth profiles for 20-nm thick TiN layers deposited under Conditions I and II. The depths were calculated from the etching time and etching rate. Ti and N compositions maintained a stoichiometric ratio in the films for both conditions I and II. This is identical to the results of in situ AES analysis, which indicated that the Ti/N ratio was 1:1 for 50 nm TiN deposited under Conditions I and II. However, for Condition II, N became rich at the TiN/Si interface. Considering that TiN film had a stoichiometric composition, the excess N at the TiN/Si interface could have been caused by the N from the amorphous interlayer. The compositions of the interlayer were mainly $SiN_x$.

The O content was constant throughout the TiN films and only a few atomic percent. There was no increase in O content at the TiN/Si interfaces. The O was mainly from the background gasses. Because the base pressure and working pressure were the same at Conditions I and II, the reason for the thick amorphous interlayer formed under Condition II was not due to the O concentration.

The TEM results also indicate that the amorphous interlayer formed under Condition II

consisted mainly of $SiN_x$ with minor Ti concentration. Figs. 2d-f show that the contrast of the interlayer was much brighter than that of the TiN layer, and closer to that of Si. This indicates that the interlayer was mainly composed of Si and N, and little Ti, because the relatively heavy Ti atoms efficiently scatter electrons, and would therefore darken the contrast of the layer if it contained high concentrations of Ti.

## IV. DISCUSSION

### A. Amorphous layer formation and crystal nucleation processes

The above results indicate that the initial growth of TiN on Si at room temperature undergoes a thickness-dependent crystal nucleation from the initial continuous amorphous layer. We qualitatively explain this phenomenon below.

At the beginning of film deposition, the deposition species of mostly Ti and N atoms and ions are arriving at the bare Si surface. Since the stoichiometric TiN can be formed for 0.015 Pa $\leq P_{N2} \leq$ 0.47 Pa, excess N-species probably arrives at Si surface compared with Ti-species for both Conditions I ($P_{N2}$ = 0.047 Pa) and II ($P_{N2}$ = 0.47 Pa). Especially under Condition II, the excess N species arriving at Si surface react with Si to from $SiN_X$ amorphous layer on it before continuous $TiN_X$ layer is formed. The main species contributing to $SiN_X$ layer formation would probably be ions such as $N_2^+$ and $N^+$ since it is known that the reaction of N atoms with Si surfaces saturates at 1-2 ML thickness while the reaction of N ions proceeds further. [16]

Then $TiN_X$ deposits are formed on Si surfaces with thin (< 0.5 nm) and thick (1.5- 1.8 nm) $SiN_X$ layers under Conditions I and II, respectively. When the film thickness is small, the contribution of deposit-surface interface to the overall Gibbs free energy of the film should be large. The interaction between $TiN_X$ deposits and amorphous $SiN_X$ may have hindered the crystallization of $TiN_X$ deposits.

As the film grows, the influence of the interfacial interaction weakens, and crystal nucleation can initiate at the upper surface of the film under the impact of the incident atoms/ions. The released crystal binding energy might promote further crystallization in the nanometer amorphous layer, and a transition from an amorphous to polycrystalline film occurs. To further understand this mechanism, studies of the deposition under various conditions, such as high substrate temperature or substrate biasing, are needed.

## B. Grain growth process

Next, we discuss the reasons for the grains being relatively broad under Condition II, and the effects on film textural evolution.

During film deposition, the energy flux onto the film or substrate is contributed by the sputtered Ti and N atoms, reflected neutral species such as Ar and N, ions such as $Ar^+$, $N_2^+$, and $N^+$, and electrons. The impinge flux of the species except Ti is much larger than that of Ti when stoichiometric TiN is deposited. This means that the energy flux onto the film or substrate may be less affected by the sputtered Ti flux. Since the deposition rate under Condition II was 1/3 of that under Condition I, the total irradiation energy per deposited atom should increase under condition II. This conjecture is identical with the results for reactive sputter deposition of AlN, [15] that the total irradiation energy per deposited atom increases significantly with increasing $N_2$ ratio. Moreover, in our sputter system, the decreased substrate self-bias potential (-23.0 V under Condition I to -29.3 V under Condition II) under Condition II may enhance the ion irradiation onto the film or substrate. The higher irradiation energy to the film has two effects on the initial film growth.

1) Higher irradiation energy increases the mobility of the adatoms on the surface of the grains, causing adatoms to diffuse to the edges.
2) When the grains grow large enough to contact each other, the higher irradiation energy

enhances coalescence and restructuring of grains.

Both the effects favor the lateral grain-growth. The grains with anisotropic planar shapes have a larger top area than side area, and tend to change into (200)-oriented grains to minimize the surface energy. This change can be realized by restructuring of the grains with a large lateral size under energetic bombardment of the incident atoms/ions, especially during coalescence.

For thick films (1.6-μm-thick), L. Hultman et al [2] found that the (200) textured TiN on $SiO_2$ consists mainly of (200) oriented columns from the TiN/substrate interface with constant diameter. This means that the (200) preferred orientation was formed during the initial stage of deposition. Our results showed that in the initial nucleation stage, the nuclei had a random orientation under Condition II, although the 50 nm thick film had a complete (200) texture. [8] The enhanced lateral grain-growth and coalescence induced restructuring of the grains into the (200) orientation, and resulted in the formation of (200) oriented columns, as observed by Hultman et al.

On the other hand, when the films were deposited under Condition I, compared with growth under Condition II, due to the lower atomic mobility and less coalescence, the grains had a lower lateral growth rate. (111) texture was formed at the film thickness of 50 nm by competition grain-growth. [8]

## V. CONCLUSIONS

We used high-resolution transmission electron microscopy (HRTEM) and nano-beam diffraction (NBD) techniques to investigate the initial growth stage of TiN thin films on (111) Si deposited by reactive magnetron dc sputtering. Initial TiN layers formed on (111) Si were continuous and amorphous at film thickness less than 1 nm. As the film thickness increased to about 2 nm, crystal nucleation occurred from the amorphous layer. The grain-growth process

was affected by the $N_2$ partial pressure, $P_{N2}$. Increasing $P_{N2}$ from 0.047 to 0.47 Pa enhanced lateral grain growth and coalescence between grains. The planar shape of the grains with large lateral size and enhanced coalescence at higher $P_{N2}$ induced restructuring of grains to thermodynamically favored (200) orientation. Compared with film deposited at a $P_{N2}$ of 0.047 Pa, for films deposited at $P_{N2}$ = 0.47 Pa a distinct amorphous interlayer (1.5-1.8 nm thick) exists between TiN layer and Si substrate. XPS and HRTEM analysis indicated this interlayer to be mainly $SiN_x$.

**ACKNOWLEDGEMENTS**

We thank Professors Y. Yamaguchi, T. Okubo, and Y. Shimogaki for helpful discussions and comments, and we thank Mr. Y. Kajikawa for advice during writing this paper. This work was supported, in part, by the New Energy and Industrial Technology Development Organization's (NEDO) "Nanotechnology Program - Systemization of Nanotechnology Materials Program Results Project", of the Ministry of Economy, Trade, and Industry (METI), Japan, and by the Japan Society for the Promotion of Science (JSPS)'s "Grant-in-Aid for Creative Scientific Research - Establishment of Networked Knowledge System with Structured Knowledge for Future Scientific Frontier Project", of the Ministry of Education, Culture, Sports, Science and Technology (MEXT), Japan.

## REFERENCES


[1]H. Onoda, M. Kageyama, and K. Hashimoto, J. Appl. Phys. **77**, 885 (1995).

[2]D.P. Tracy, D.B. Knorr, and K.P. Rodbell, J. Appl. Phys. **76**, 2671(1994).

[3]D.B. Knorr, S.M. Merchant, and M.A. Biberger, J. Vac. Sci. Technol. B **16**, 2734 (1998).

[4]L. Hultman, J.-E. Sundgren, J. E. Greene, D. B. Bergstrom, and I. Petrov, J. Appl. Phys. **78**, 5395 (1995).

[5]J.-S. Chun, I. Petrov, and J. E. Greene, J. Appl. Phys. **86**, 3633 (1999).

[6]U. C. Oh, J. H. Je, and J. Y. Lee, J. Mater. Res. **13**, 1225 (1998).

[7]J. Pelleg, L. Z. Zevin, S. Lungo, and N. Croitoru, Thin Solid Films **197**, 117 (1991).

[8]T. Q. Li, S. Noda, Y. Tsuji, T. Ohsawa, and H. Komiyama, J. Vac. Sci. Technol. A **20**, 583 (2002).

[9]F.H. Baumann, D.L. Chopp, T. Diaz de la Rubia, G.H. Gilmer, J.E. Greene, H. Huang, S. Kodambaka, P.O'Sullivan, and I. Petrov, MRS Bull. **26**, 182 (2001).

[10]S. Kodambaka, V. Petrova, A. Vailionis, P. Desjardins, D.G. Cahill, I. Petrov, J.E. Greene, Thin Solid Films, **392**, 164 (2001).

[11]S. Kodambaka, V. Petrova, S.V. Khare, D. Gall, A. Rockett, I. Petrov, J.E. Greene, Phys. Rev. Lett. **89**, 176102-1 (2002).

[12]S. P. Murarka, R. J. Gutmann, A. E. Kaloyeros, and W. A. Lanford, Thin Solid Films **236**, 257 (1993).

[13]P. Patsalas and S. Logothetidis, J. Appl. Phys. **93**, 989 (2003).

[14]M.J. Williamson, D.N. Dunn, R. Hull, S. Kodambaka, I. Petrov, and J.E. Greene, Appl. Phys. Lett. **78**, 2223 (2001).

[15]T.P. Drüsedau, K. Koppenhagen, J. Bläsing, T.-M. John, Appl. Phys. A **72**, 541 (2001).

[16]Takuya Seino, Takashi Matsuura, and Junichi Murota, Appl. Phys. Lett. **76**, 342 (2000).

Table I TiN deposition conditions

| | Condition I | Condition II |
|---|---|---|
| Discharge power (W) | dc 69 | |
| Working pressure (Pa) | 0.93 | |
| $N_2$ partial pressure (Pa) | 0.047 | 0.47 |
| Deposition rate (nm/s) | 0.19 | 0.063 |

**FIGURE CAPTIONS**

Fig. 1 Plan-view TEM images and corresponding SAED patterns of TiN deposited under Condition I for deposition times of (a) 4 s, (b) 10 s, and (c) 30 s, and under Condition II for deposition times of (d) 10.5 s, (e) 32 s, and (f) 60 s.

Fig. 2 Cross-sectional TEM images of TiN deposited onto (111) Si substrates under Condition I for deposition times of (a) 4 s, (b) 10 s, and (c) 30 s, and under Condition II for deposition times of (d) 10.5 s, (e) 32 s, and (f) 60 s.

Fig. 3 NBD patterns of cross-sectional samples of (a) film formed under Condition I for a deposition time of 4 s, (b) Si substrate, and (c) film formed under Condition I for a deposition time of 10 s.

Fig. 4 Frequency histograms of TiN lateral grain dimension for samples deposited under (a) Condition I and under (b) Condition II.

Fig. 5 Lateral grain growth vs. film thickness.

Fig. 6 Enlarged plan-view HRTEM images of grains taken from Fig. 1c, (a)-(d), and Fig. 1f, (e)-(h), corresponding to the marked grains 1-4 in Figs. 1c and f, respectively.

Fig. 7 XPS depth profiles of 20-nm thick TiN layers deposited under Conditions I (a) and II (b).

Fig. 1

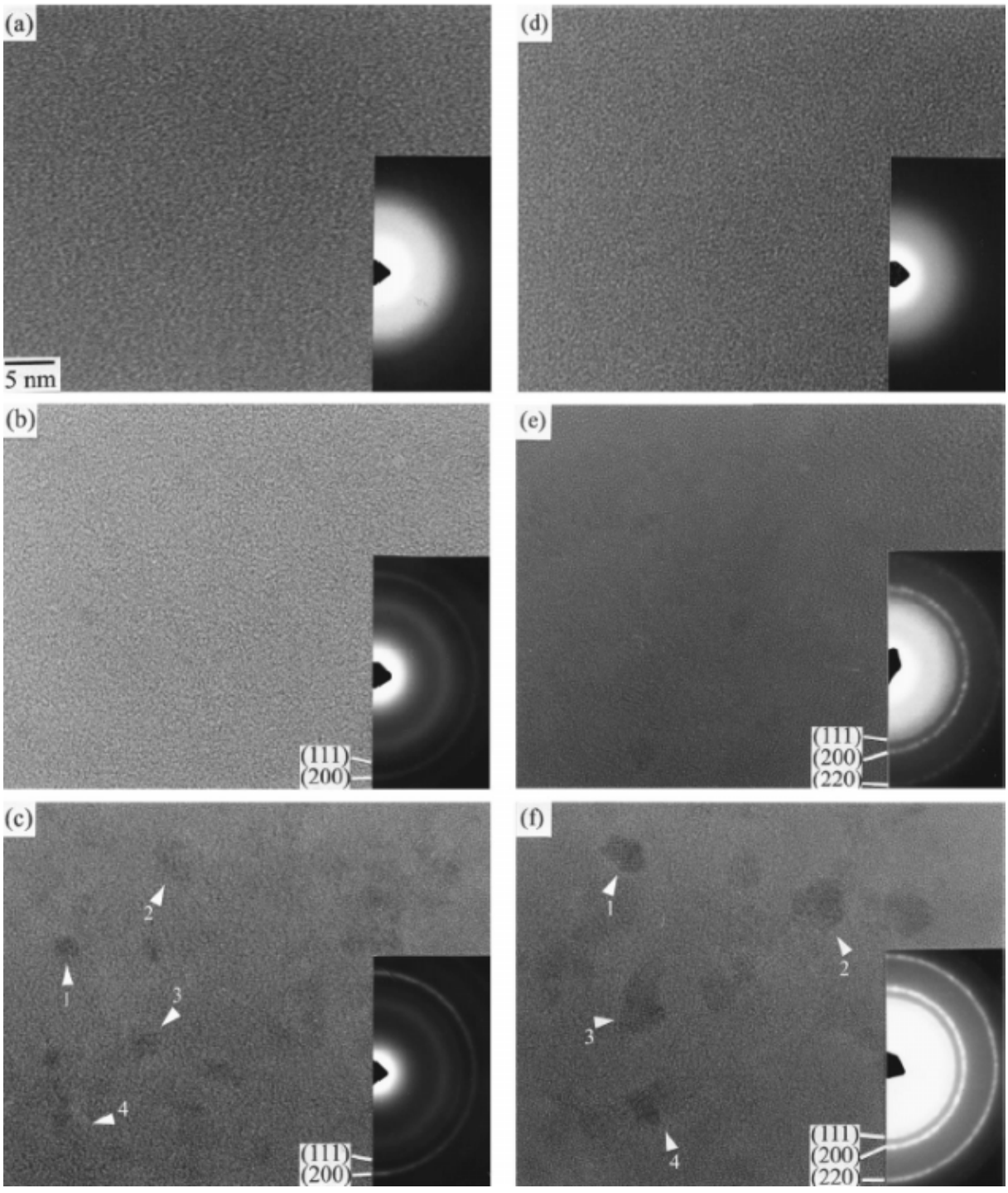

Fig. 2

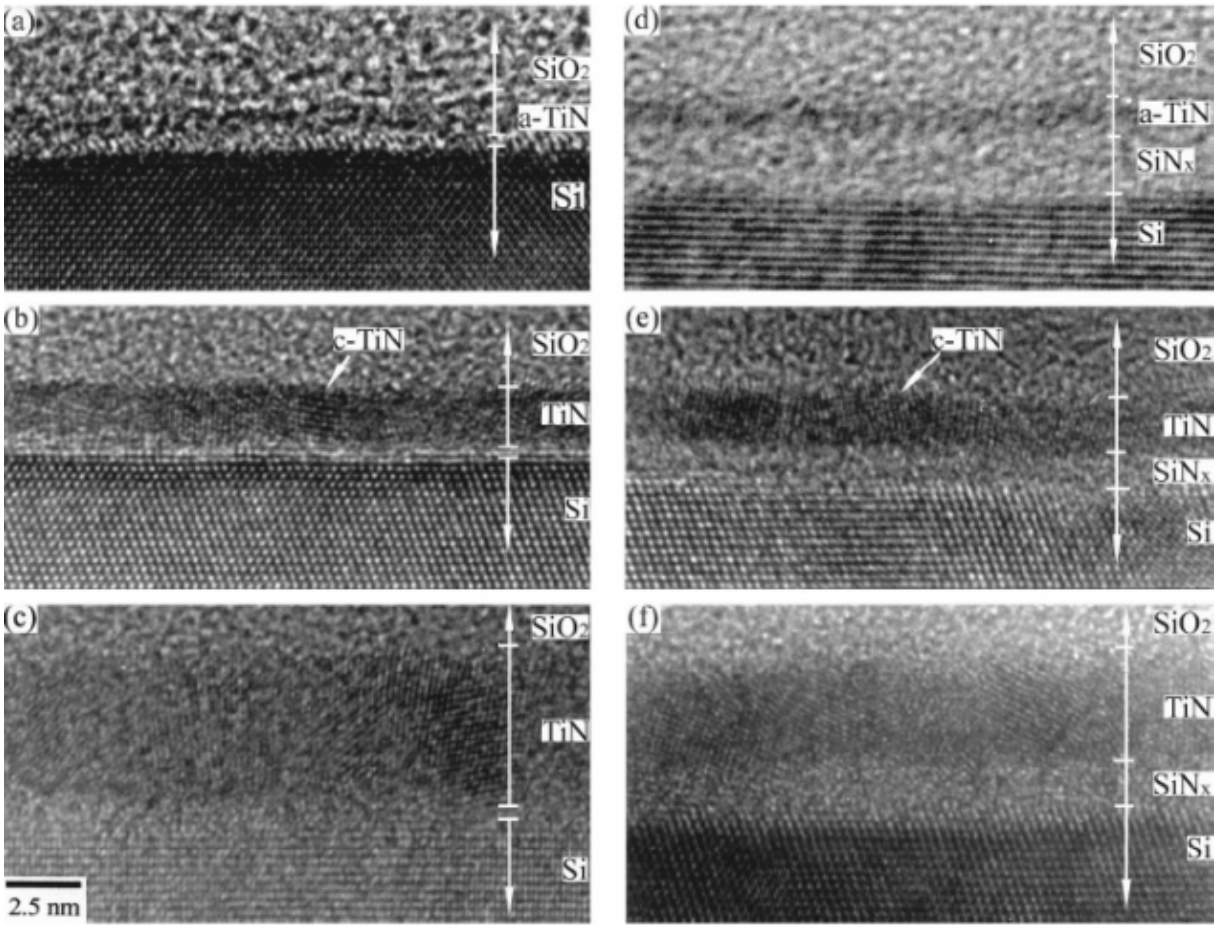
(a)
SiO2
a-TiN
Si
(d)
SiO2
a-TiN
SiNx
Si
(b)
c-TiN
SiO2
TiN
Si
(e)
c-TiN
SiO2
TiN
SiNx
Si
(c)
SiO2
TiN
Si
2.5 nm
(f)
SiO2
TiN
SiNx
Si

Fig. 3

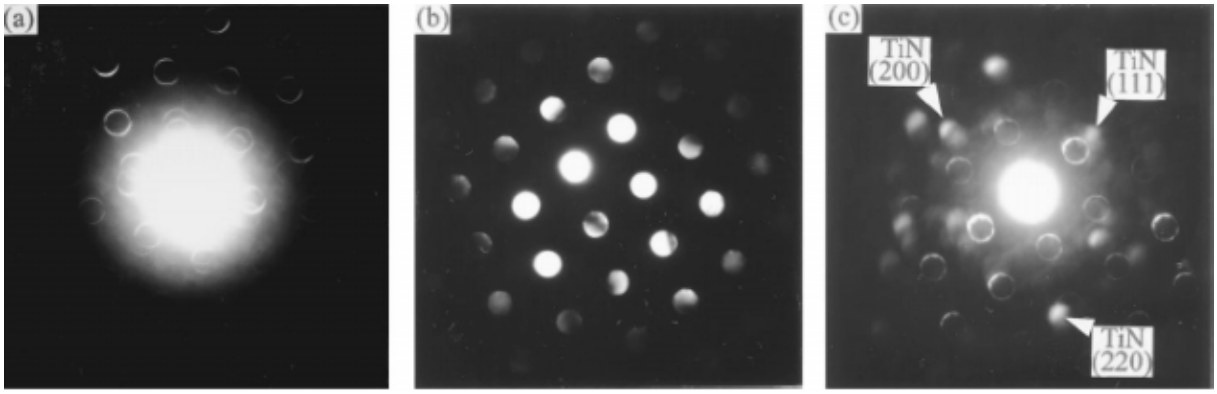

Fig. 4

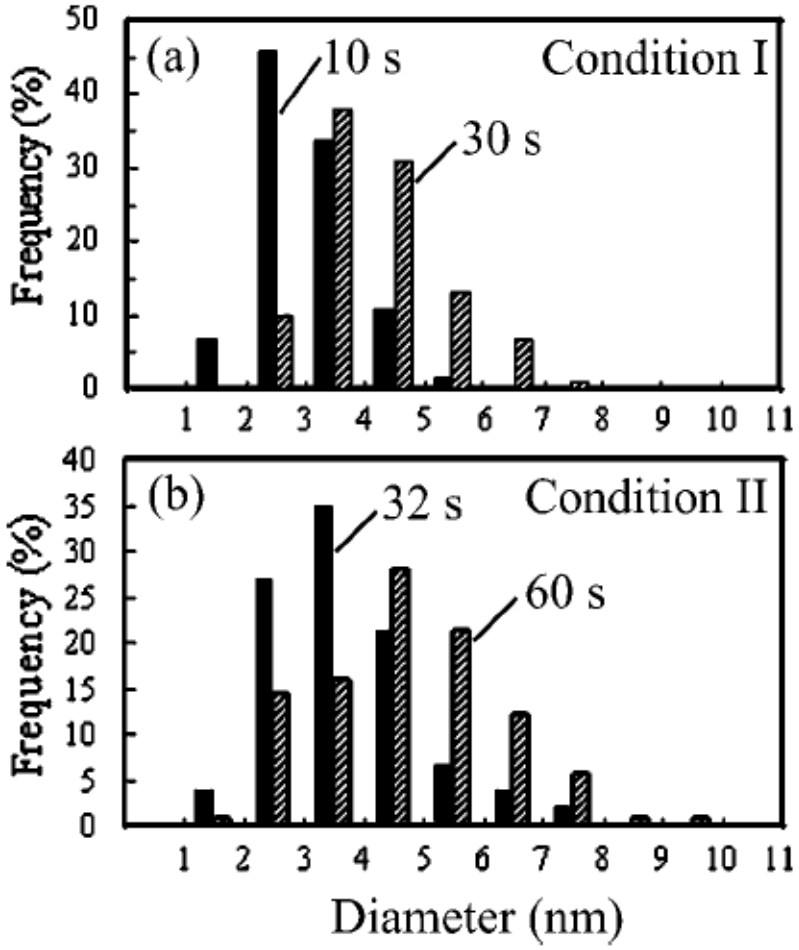
(a)
10 s
30 s
Condition I
Frequency (%)
(b)
32 s
60 s
Condition II
Frequency (%)
Diameter (nm)

Fig. 5

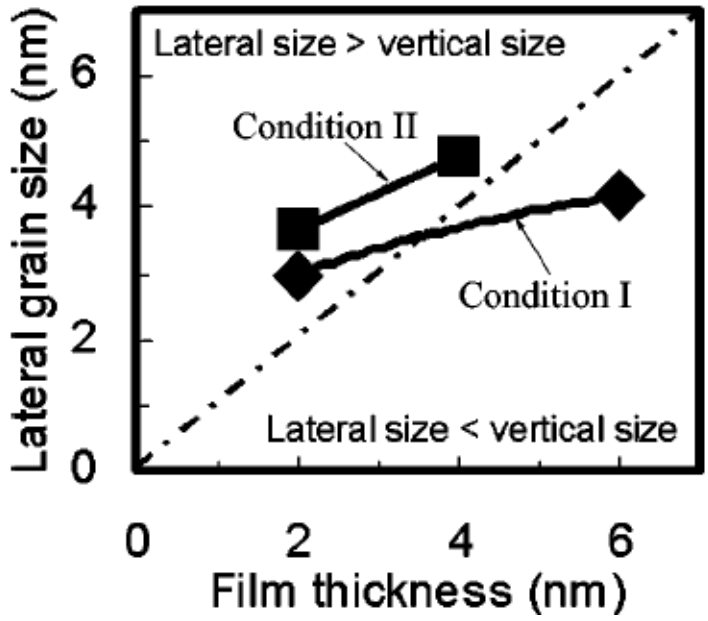
Lateral size > vertical size
Condition II
Condition I
Lateral size < vertical size
Lateral grain size (nm)
0
2
4
6
0
2
4
6
Film thickness (nm)

Fig. 6

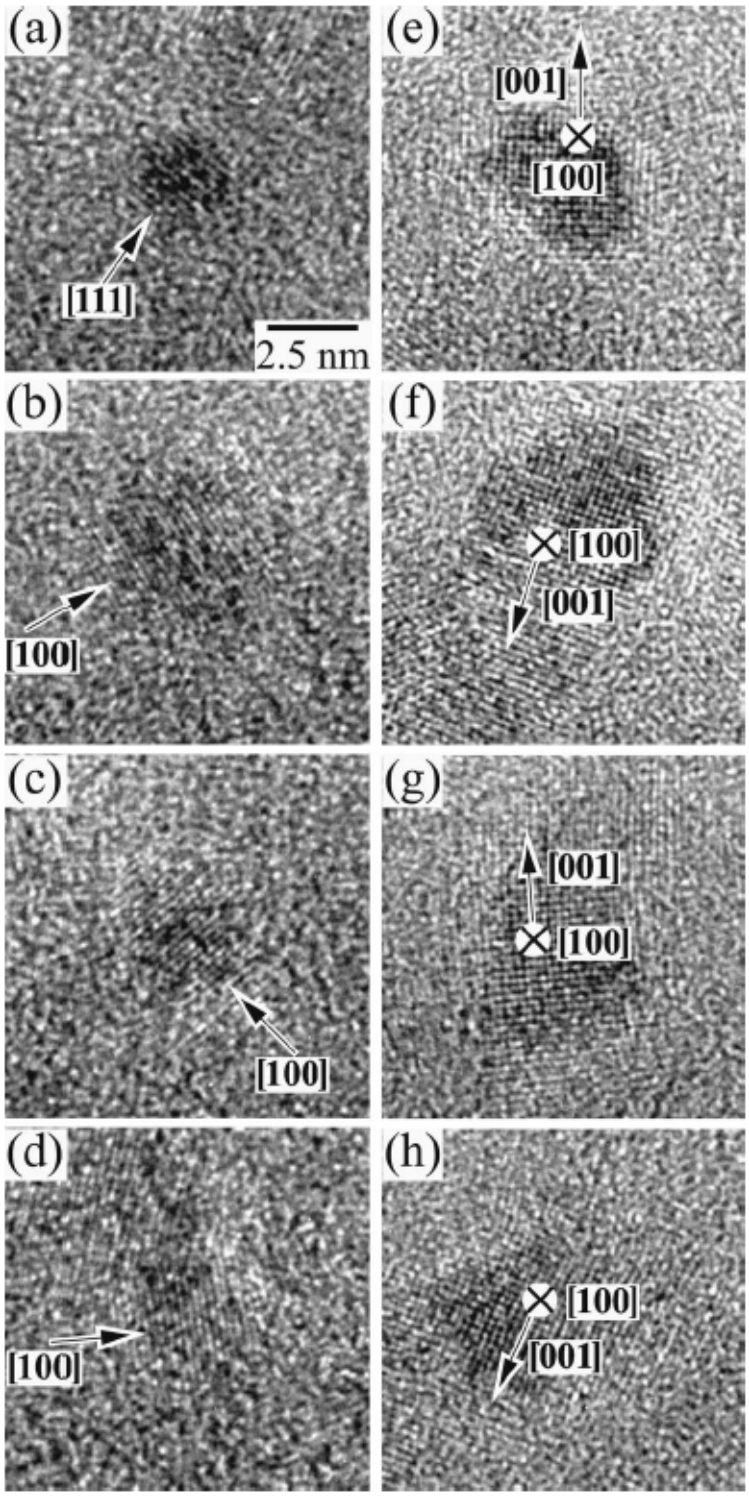

Fig. 7

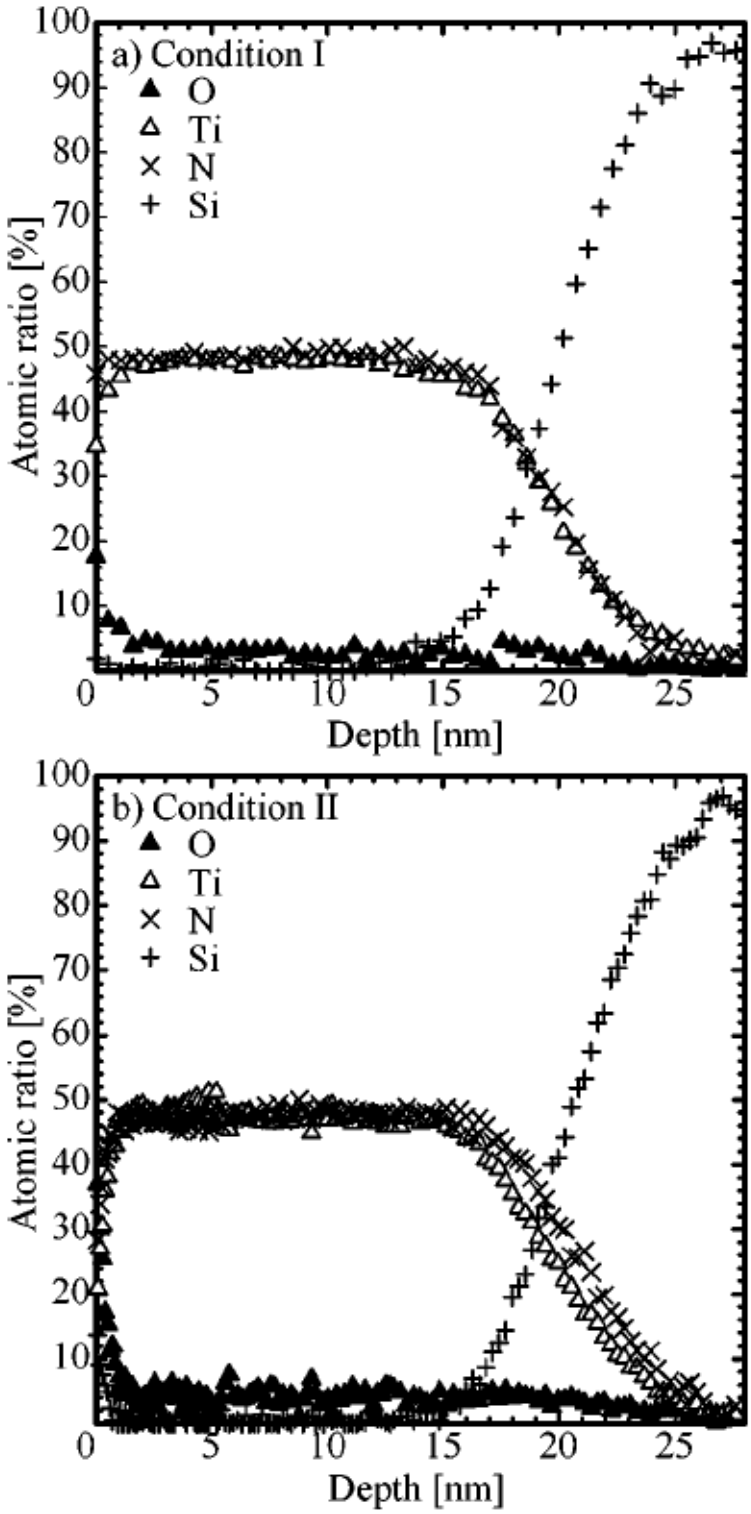
a) Condition I
O
Ti
N
Si
Atomic ratio [%]
Depth [nm]
b) Condition II
O
Ti
N
Si
Atomic ratio [%]
Depth [nm]